Applied Physics Letters

# Magneto-thermal transport indicating enhanced Nernst response in FeCo/IrMn exchange coupled stacks

Cite as: Appl. Phys. Lett. **121**, 212405 (2022); https://doi.org/10.1063/5.0113485
Submitted: 23 July 2022 • Accepted: 07 November 2022 • Published Online: 21 November 2022

Mickey Martini, Helena Reichlova, Yejin Lee, et al.







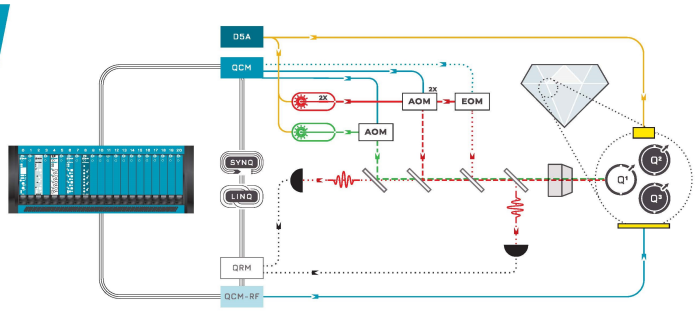

Applied Physics Letters ARTICLE scitation.org/journal/apl

# Magneto-thermal transport indicating enhanced Nernst response in FeCo/IrMn exchange coupled stacks

Cite as: Appl. Phys. Lett. **121**, 212405 (2022); doi: 10.1063/5.0113485
Submitted: 23 July 2022 · Accepted: 7 November 2022 ·
Published Online: 21 November 2022



Mickey Martini,[1,2,a)] Helena Reichlova,[3,4] Yejin Lee,[1,2] Dominika Dusíková,[5] Jan Zemen,[5] Kornelius Nielsch,[1,2,6] and Andy Thomas[1,4]

## AFFILIATIONS

[1]Leibnitz Institute for Solid State and Materials Science Dresden (IFW Dresden), 01069 Dresden, Germany
[2]Institute of Applied Physics, Technische Universität Dresden, 01062 Dresden, Germany
[3]Institute of Physics of the Czech Academy of Sciences, Na Slovance 1999/2, 18221 Prague, Czech Republic
[4]Institut für Festkörper- und Materialphysik, Technische Universität Dresden, 01069 Dresden, Germany
[5]Faculty of Electrical Engineering, Czech Technical University, Technicka 2, 16627 Prague, Czech Republic
[6]Institute of Materials Science, Technische Universität Dresden, 01062 Dresden, Germany

[a)]**Author to whom correspondence should be addressed:** m.martini@ifw-dresden.de

## ABSTRACT

We present an analysis of magneto-thermal transport data in IrMn/FeCo bilayers based on the Mott relation and report an enhancement of the Nernst response in the vicinity of the blocking temperature. We measure all four transport coefficients of the longitudinal resistivity, anomalous Hall resistivity, Seebeck effect, and anomalous Nernst effect, and we show a deviation arising around the blocking temperature between the measured Nernst coefficient and the one calculated using the Mott rule. We attribute this discrepancy to spin fluctuations at the antiferromagnet/ferromagnet interface near the blocking temperature. The latter is estimated by magnetometry and magneto-transport measurements.



Exchange coupling between ferromagnetic (FM) and antiferromagnetic (AFM) layers leads to a shift in the hysteresis loop of a ferromagnet and/or its broadening. This unidirectional pinning of the FM layer is important for technological applications and, consequently, it is exploited in spintronic devices, such that spin valves,[1–3] magnetic tunnel junctions,[4–12] and domain wall nano wires.[13] Various models of exchange bias have been discussed,[14–16] and the ways of detecting and manipulating the exchange coupling effect are actively studied on the fundamental research level.[17–23]

Widely used AFM material systems for exchange bias are bilayers of IrMn/FeCo, because they exhibit a robust shift of the hysteresis loop and a reversible unidirectional pinning of the FM by cooling in the magnetic field with opposite polarities. Moreover, the blocking temperature ($T_B$) is the temperature below which the FM and AFM layers are coupled, and the Néel temperature can be tuned by the thickness of IrMn to be below room temperature.[24–26]

The exchange coupling has experimentally been measured by magnetometry,[27,28] Kerr effect,[17,29,30] magnetization-induced second harmonic generation,[31] or magneto-transport.[32,33] From the application perspective, the transport detection is the most desirable. With the renewed interest in the anomalous Nernst effect,[34] the detection of the exchange bias via magneto-thermal transport effects is also studied. It was shown that the exchange coupling can be also detected thermally[35] and the recently recorded thermopower was experimentally and theoretically reported in exchange bias stacks.[24,36] A systematic study of one set of exchange bias stacks by magnetometry, magneto-transport, and magneto-thermal transport is, however, missing. Similarly, the Mott relation which links the electrical (resistance and Hall effects) and thermoelectric transport coefficients (Seebeck and Nernst effects) was not studied. The validity of Mott formula has been explored in a variety of materials, such as spinels,[37] diluted magnetic semiconductors,[38] topological materials,[39–41] semicrystalline polymers,[42] and van der Waals systems.[43]

Here, we report a series of exchange coupled samples Ta/IrMn($t$)/FeCo, where the thickness $t$ of the antiferromagnet was varied between 1 and 3 nm. The samples are systematically studied in the

temperature range of 10–300 K by magnetometry and magnetotransport and a robust exchange bias can be observed. The blocking temperature is estimated by both methods. The sample with a thicker IrMn layer is also studied by magneto-thermal transport. Although the measured anomalous Nernst and magneto Seebeck data do not directly show signatures of exchange bias, our analysis based on the four magneto-thermal transport coefficients reveals deviation from the Mott relation in the vicinity of the blocking temperature probably arising from the spin fluctuation on the FM and AFM interface.[44]

We grow Ta(5)/IrMn(1–3)/FeCo(3) multilayers with in-plane magnetic anisotopy on magnesia substrates by DC magnetron sputtering at room temperature (numbers indicate the thickness in nm). While a Ta buffer layer is conventionally used as a seed layer to increase the exchange coupling[26,45] and to introduce an atomically smooth interface,[46] it increases the conductivity and, therefore, slightly changes the distribution of the current density in the multilayer. For all samples, an MgO capping layer of 3 nm is used to prevent oxidation. The base and Ar sputtering pressures of the deposition chamber are $2 \times 10^{-9}$ and $3 \times 10^{-3}$ mbar, respectively. The full series, illustrated in Fig. 1(a), is aimed to study the temperature and thickness dependence of the exchange–coupling effect and the magnetic coercivity. The multilayers are cooled down in a magnetic field of 7 T between 300 and 10 K. The magnetization curves are recorded at different temperatures (within the 10–300 K range) with an in-plane field sweep in a superconducting quantum interference device. The measurements are repeated after a field cooling (FC) with opposite field polarity.

In Fig. 1(b), we plot representative magnetization curves taken at 100 K in Ta/IrMn(3)/FeCo/MgO. Both sets of data show open hysteresis loops, indicative of strong in-plane anisotropy. The magnetization loops are symmetrically shifted due to the unidirectional exchange anisotropy (exchange bias), which results from the exchange coupling at the FM/AFM interface below $T_B$. As depicted in the inset of Fig. 1(b), the exchange-bias field ($H_{ex}$) has the same amplitude after the two different coolings and decreases with temperature until it vanishes at approximately $T_B$. Qualitatively, the same temperature dependence of $H_{ex}$ is observed in the other multilayers [Fig. 1(c)], with a reduced $T_B$ in multilayers with thinner IrMn layer, in the agreement with the previous studies.[24,47,48] Similarly, the coercive field shows a strong temperature dependence [Fig. 1(d)]; however, the critical temperatures at which the exchange broadening and exchange shift vanish do not coincide and three different areas can be distinguished in structures with reduced $T_B$. At low temperature, the rigid AFM pins the FM, whose moments are oriented by the external field $H$, resulting in large exchange-bias effect and coercivity. When the temperature crosses $T_B$ from below, no exchange-bias is observed. However, the AFM with weak anisotropy is still coupled with the FM and the two layers follow the external magnetic field $H_{ext}$ together,[49] leading to a finite magnetic broadening. Well above $T_B$, there should be no interaction between the AFM and FM, which means no exchange broadening and exchange shift. The last area is not observed in the applicable temperature range when $t_{IrMn} \geq 2$ nm, due to high $T_B$.

The unidirectional exchange anisotropy can be also investigated by magneto-transport measurements.[50] To this end and to quantify the four transport coefficients of the longitudinal resistivity, anomalous Hall resistivity, magneto Seebeck coefficient, and anomalous Nernst coefficient in Ta(5)/IrMn(3)/FeCo(3), we use the device shown in Fig. 2(a), also indicating our coordinate system. The as-grown films are patterned into Hall bars by standard optical lithography. The heaters and thermometers are defined by optical lithography and a lift-off process with 90 nm of sputtered Pt. The temperature dependence of

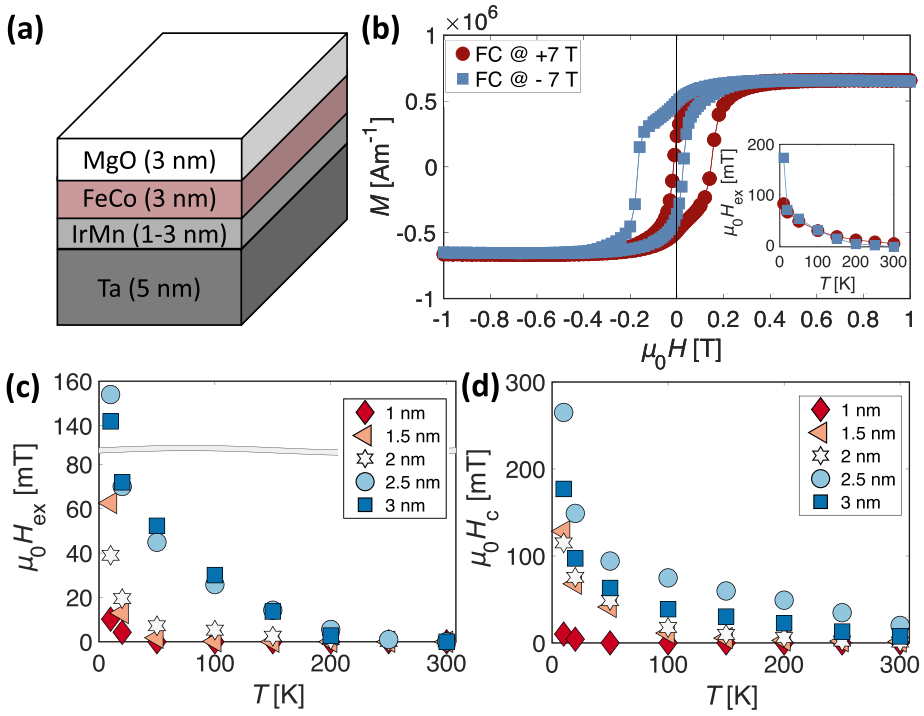


**FIG. 1.** (a) Schematic illustration of multilayer heterostructures. (b) Magnetization curves at 100 K and exchange-bias field vs temperature (inset) of Ta/MnIr(3)/FeCo/MgO after a field cooling with ±7 T. (c) Exchange-bias field vs temperature. (d) Coercive field vs temperature in all multilayers.

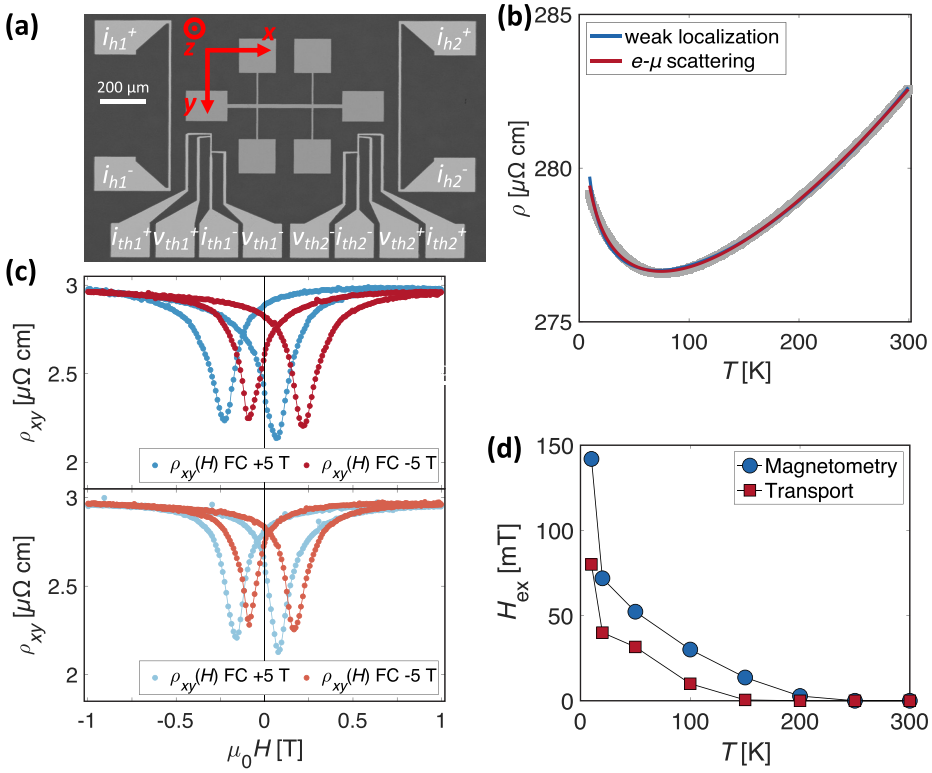


**FIG. 2.** (a) Optical image of the device and coordinate system. (b) Electrical resistivity vs temperature (gray markers). The blue and red fitting curves were calculated using the weak localization and electron-magnetic impurity scattering effects models, respectively. (c) Transversal resistivity vs in-plane field applied at 45° from the current line at 10 (top panel) and 20 K (bottom panel). (d) Comparison of exchange bias estimated by magnetometry techniques and electrical transport measurements.

the electrical resistivity measured using a four point geometry [Fig. 2(b)], estimated by considering only the conduction through Ta, IrMn, and FeCo and neglecting the contribution from the capping layer, displays a minimum between 50 and 100 K, which can be explained in terms of electron-magnetic impurities scattering effects and/or electron localization.[51–53] The data are fitted using two models: the first gives a logarithmic temperature dependence of the resistivity $\rho \propto -A \log T + BT^n$, while the second mechanism gives $\rho \propto C/\sqrt{T} + DT^m$. As shown in Fig. 2(b), the experimental data are well reproduced for both models, making impossible, based only on the electrical characterization, to identify the physical phenomenon responsible of the upturn in the temperature dependence of the resistivity in our sample. The room-temperature resistivity is enhanced of more than one order of magnitude compared to the bulk resistivity of tantalum ($\rho_{\mathrm{Ta}} = 13.1\ \mu\Omega$cm) or iron ($\rho_{\mathrm{Fe}} = 9.7\ \mu\Omega$cm) due to the increase in surface scattering in a thin multilayer.

The exchange bias is estimated by measuring the planar Hall resistivity with a field sweep after two field coolings at $\pm 5$ T, respectively. The planar transversal resistivity can be calculated as $\rho_{xy}(H) = [\rho_{\parallel} - \rho_{\perp}] \sin 2\varphi(H)$, where $\rho_{\parallel}$ ($\rho_{\perp}$) is the resistivity for current oriented parallel (perpendicular) to the magnetization and $\varphi$ is the angle between the current and magnetization axes. Figure 2(c) depicts the representative transversal resistivity taken at 10 and 20 K when the magnetic field is applied in-plane at an azimuthal angle of 45° with respect to the current line, during both cooling and measurements. At high field, $\rho_{xy}$ reaches a maximum due to the fully saturated magnetization along the field direction and $\rho_{\parallel} > \rho_{\perp}$. As the amplitude of the field is decreased, the magnetization is no longer rigidly aligned at 45° (or −135° when the field is reversed) from the current direction, with a consequent drop of $\rho_{xy}$. The presence of two peaks is explained by the application of the external field along the easy axis. The exchange bias is quantified considering the shift of the symmetry axis of $\rho_{xy}$ from the $y$ axis and is compared in Fig. 2(d) with the shift of the magnetization curve of Fig. 1(b). The two curves scale similarly with temperature; however, the exchange shift and the blocking temperature recorded by magnetotransport measurements are slightly different from the ones measured with magnetometry techniques. This discrepancy might be associated with the different thickness of the layers (thinner layers) in the Hall bar device compared with the stack of continuous films, and due to the different experimental conditions, e.g., an electrical current is flowing through the sample used for magnetotransport studies. Moreover, $\rho_{xy}$ and $M(H)$ have a different behavior because the Hall effect is very sensitive to the FeCo/IrMn interface, but the magnetization loops probe the whole stack, hence the full volume of FeCo, but not the conductive antiferromagnetic IrMn.

The coefficients of the anomalous Hall and the longitudinal resistivity are quantified by injecting a dc current with a density of $j \simeq 1 \times 10^5$ A/cm$^2$ along the $x$ axis with both polarities, and the antisymmetric component of the voltage is simultaneously measured along the $y$ and $x$ axes, during a field sweep along the $z$ axis. Figure 3(a) reports several $\rho_{xy}$ curves taken at different temperatures. A strong anomalous contribution to the Hall signal is visible around zero magnetic field, whereas the ordinary Hall effect appears as a linear slope of $\rho_{xy}$ at higher fields. The hysteresis particularly visible at lower temperatures is due to a small magnet misalignment in our cryostat that results in a finite in-plane field component during an out-of-plane sweep.

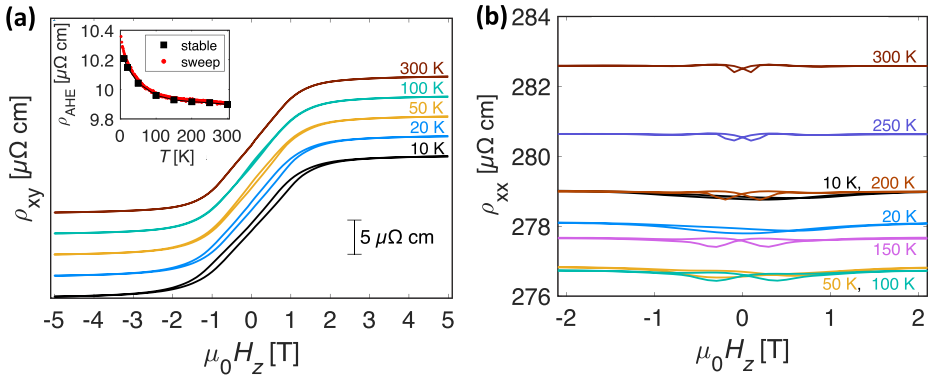


**FIG. 3.** (a) Out-of-plane field sweep of Hall resistivity at different temperatures. Inset: AHE at different temperatures and obtained with a temperature sweep at ±5 T. (b) Longitudinal resistivity as a function of out-of-plane magnetic field at different temperatures.

The anomalous Hall effect ($\rho_{\mathrm{AHE}}$) is quantified from the curves of [Fig. 3(a)] as half of the amplitude of $\rho_{xy}$ after subtracting the linear ordinary Hall background. We also quantify $\rho_{\mathrm{AHE}}$ by sweeping the temperature from 300 to 5 K in a static field of ±5 T and considering again half of the voltage difference without the ordinary contribution. As shown in the inset of Fig. 3(a), $\rho_{\mathrm{AHE}}$ slightly varies with temperature. This feature can be explained by reminding that in poorly conducting regime ($\rho_{xx} > 100\ \mu\Omega$cm), the intrinsic contribution of the AHE is damped and only the skew scattering mechanism is present.[54,55] The latter is related to the amplitude of the total magnetization,[54] which is expected to slightly decrease in our sample in the studied temperature range.

The longitudinal resistivity is depicted in Fig. 3(b). As usual in magnetic multilayers, the system shows a positive magnetoresistance effect at low field, due to a helical path induced by the Lorentz force, which in turn results in a reduction in the mean free path. At high field ($\mu_0 H_z > 1$ T), the magnetization is fully saturated along the field direction and the longitudinal resistivity remains constant. The hysteretic behavior observable around zero field is also due to the magnetic field misalignment.

To study the thermomagnetic response of the magnetic multilayer, we generate a temperature gradient ($\nabla T$) along $x$ direction by driving a constant current through the on chip heater lines [see Fig. 2(a)]. The temperature gradient is assumed spatially uniform and estimated as $\nabla T = (T_1 - T_2)/l$, where $T_1$ and $T_2$ denote the temperatures on the cold and hot sides of the sample, monitored by the on-chip thermometers, and $l = 620\ \mu$m quantifies the distance between the two thermometers. The resistance of each thermometer as a function of the base temperature is shown in Fig. 4(a), along with the two thermometers' resistances measured at some specific temperatures while a current of 30 mA is injected through the heating line. The calibration curves (black and gray lines) are used to map the thermometer resistance onto corresponding temperature when one side of the device is heated up, to quantify the thermal gradient. In the inset of Fig. 4(a), we report $\nabla T$ at different temperatures for $i_h = 30$ mA. The temperature profile of the sample is also simulated with finite element methods at base temperatures of 100 and 300 K and $i_h = 30$ mA. We find that $\nabla T$ is highly dependent on the base temperature, as experimentally demonstrated, and decreases by a factor of 2–3 between the hot and cold regions of the Hall bar, regardless of the base temperature. By means of this simulation, we notice that the presence of intermediate structures between the heaters lines has no effect on the temperature profile. The simulated $\nabla T$ also strongly depends on the electrical conductivity of the heater, and we obtain a thermal gradient in quantitative agreement with the experimental estimate for heater conductivity which is one half of that of bulk Pt. This means that the nominal values and the real values of the thermal gradient and, hence, the absolute values of the thermal transport coefficients that depend on it, could differ by a factor of 2–3. Nevertheless, this difference applies equally to all base temperatures and has no impact on our study, based on relative changes of the thermal coefficients over temperature. To estimate the magneto Seebeck and Nernst effects, we sweep the magnetic field along the $z$ axis, and measure the voltage drop along the $x$ and $y$ axes, while a dc current is injected through the heater line. The Seebeck (Nernst) coefficient is the diagonal (off diagonal) tensor element and can be approximated to an even (odd) function of the magnetic field. We take advantage of this property to symmetrize the longitudinal voltage ($V_{xx}$) and antisymmetrize the transversal voltage ($V_{xy}$) with respect to the magnetic field to decouple magneto Seebeck and Nernst effects, which are otherwise weakly mixed due to the geometry of the thermal gradient, which is not exactly parallel to $x$. In Figs. 4(b) and 4(c), we show representative symmetrized longitudinal and antisymmetrized transversal voltages measured for different heating current amplitudes ($i_h$ = 17–30 mA) at 300 K. For our analysis, we consider the voltages measured using the same pairs of contacts at different temperatures, since $\nabla T$ is not completely constant over the Hall bar region. At each temperature, we plot $V_{xx}$ at 5 T and the amplitude of the anomalous Nernst effect $V_{ANE}$ vs the thermal gradient associated with the heating current amplitude, and we perform a linear fit to extract the magnetothermal coefficients, as shown in Fig. 4(d) for $T$ = 300 K. The magneto Seebeck coefficient ($S_{xx}$) is evaluated by normalizing the slope of the fitting line by the length over which $V_{xx}$ is detected, whereas the anomalous Nernst coefficient ($S_{ANE}$) is determined dividing the slope of the corresponding fitting line by the contact y-spacing. As depicted in Fig. 4(e), $S_{xx}$ increases monotonously from 1.4 $\mu$V K$^{-1}$ to $S_{xx} = 6.5\ \mu$V K$^{-1}$ when the temperature is raised from 120 to 300 K. Conversely, $S_{ANE}$ shows a clear peak around 150 K [Fig. 4(f)], which is the critical temperature at which the exchange coupling between FM and AFM layers of the device determined by transport measurement vanishes [see Fig. 2(d)].

The four measured thermoeletric coefficients are employed to check the applicability of Mott relation[56] in our FM/AFM multilayer in a range of temperatures that includes the antiferromagnetic transition (120–300 K). Pu *et al.* demonstrate that, under the general

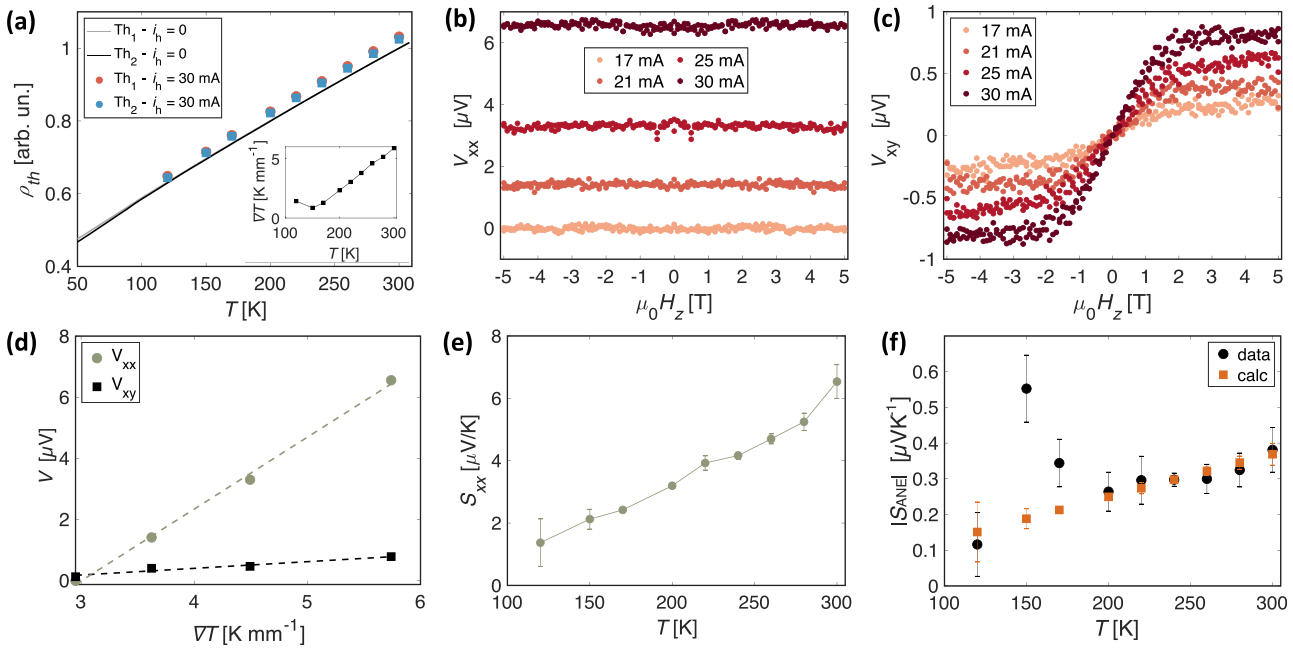


**FIG. 4.** (a) Calibration curves of the Pt thermometers vs base temperature of the cryostat. The calibration curves without heating are interpolated to extract the thermometer temperature for a given resistance. The red and blue markers denote the resistance of Th1 (hot side) and Th2 (cold side) measured at some specific base temperatures during homogeneous heating of the sample ($i_h = 30$ mA). Inset: Temperature gradient as a function of base temperature for $i_h = 30$ mA. (b) Magnetic thermopower as a function of the magnetic field at 300 K for different heating current amplitudes. (c) Nernst effect vs external field applied out-of-plane for different heating current amplitudes. (d) Longitudinal and transversal voltages measured at 5 T vs thermal gradient. The dashed lines represent the fitted linear regression curves. (e) Magneto Seebeck coefficient as a function of base temperature. (f) Measured and calculated ANE at different temperatures.

assumption of a simple power law dependence $\rho_{AHE} = \lambda M_z \rho_{xx}^n$, the Mott relation involves only these four transport coefficients[38]

$$|S_{\mathrm{ANE}}^{calc}| = \left| \frac{\rho_{\mathrm{AHE}}}{\rho_{xx}} \left( \frac{\pi^2 k_B^2}{3e} \frac{\lambda'}{\lambda} T - (n-1) S_{xx} \right) \right|, \quad (1)$$

where $\lambda'/\lambda$ and $n$ are, respectively, the prefactor and exponent of the power law ansatz, both temperature-independent. It is worth notice that in contrast to the power law assumption, Eq. (1) does not involve the magnetization. The magnetization is estimated by magnetometry on a different sample with a size of three orders of magnitude larger than the device used for transport measurements. This would inevitably cause error in the power law analysis. Equation (1) includes, instead, only magneto-thermal transport coefficients determined on the same sample. In Eq. (1), we fix $n = 1$, assuming that the AHE is dominated by the extrinsic contribution ($\rho_{AHE} \propto M_z \rho_{xx}$) and treated $\lambda'/\lambda$ as one parameter. Figure 4(f) represents the curve calculated from Eq. (1) for $\lambda'/\lambda = 8.96 \times 10^{18}\ \mathrm{J}^{-1}$, along with the measured curve. At low and high temperatures, the experimental data are well reproduced by the calculated coefficient; however, a discrepancy between the two curves arises around 150 K, where the antiferromagnetic transition occurs, and persists even if $n$ is varied between 1 and 2. To support our analysis and conclusion, we also employ the four magneto-thermal transport coefficients to estimate the anomalous Nernst conductivity by taking advantage of the second Mott equation[38] and compare the calculated curve with the Nernst conductivity estimated as[57,58] $\alpha_{yx} = (S_{xx}\rho_{xy} + S_{yx}\rho_{xx})/(\rho_{xx}^2 + \rho_{xy}^2)$. The Mott relation to calculate the Nernst conductivity is

$$|\alpha_{yx}^{calc}| = \left| \frac{\rho_{yx}}{\rho_{xx}^2} \left( \frac{\pi^2 k_B^2}{3e} \frac{\lambda'}{\lambda} T - (n-2) S_{xx} \right) \right|. \quad (2)$$

In Eq. (2), we use the same set of parameters $\lambda'/\lambda$ and $n$ as in Eq. (1). Then, we get measured and calculated Nernst conductivities overlapping each other, with a deviation around the blocking temperature. These two curves are very similar to the measured and calculated Nernst coefficients of Fig. 4(f), respectively, and are consequently not depicted. The violation of the Mott relation might be due to enhanced electron–magnon collisions around the blocking temperature. The simplified Mott formula is in fact valid only if the charge carriers are scattered dominantly by impurities and lattice defects, whereas it does not take into account nondiffusive mechanisms, such that phonon or magnon drag.[59,60] In conclusion, we study the temperature dependence of the magneto-thermal transport properties of IrMn/FeCo exchange coupled multilayers. Systematic measurements of $M(H)$ hysteresis loops reveal that the unidirectional exchange anisotropy arising at FeCo/IrMn interface after a field cooling leads to a robust exchange shift and sizeable broadening in our FM/AFM stacks. This conclusion is also supported by planar Hall measurements performed in Ta(5)/IrMn(3)/FeCo(3). Moreover, we confirm that the blocking temperature can be tuned to be below room temperature by adjusting the thickness of the IrMn layer, which can be influenced by grains at the IrMn/CoFe. The four transport coefficients of longitudinal resistivity,

anomalous Hall resistivity, magneto-Seebeck, and anomalous Nernst coefficients are extracted from out-of-plane magnetic field measurements. Our analysis based on the four magneto-thermal transport coefficients reveals a deviation from the Mott relation in the vicinity of the blocking temperature. We attribute this possible violation of the Mott formula to the spin fluctuation at the IrMn/FeCo interface in the vicinity of the blocking temperature.

## AUTHOR DECLARATIONS

### Conflict of Interest

The authors have no conflicts to disclose.

### Author Contributions

**Mickey Martini:** Data curation (lead); Formal analysis (lead); Investigation (lead); Methodology (supporting); Software (equal); Writing – original draft (lead); Writing – review & editing (lead). **Helena Reichlova:** Software (supporting); Supervision (supporting); Validation (supporting); Writing – original draft (supporting). **Yejin Lee:** Investigation (supporting); Methodology (lead). **Dominika Dusíková:** Validation (equal); Writing – review & editing (equal). **Jan Zemen:** Data curation (equal); Validation (equal); Writing – review & editing (equal). **Kornelius Nielsch:** Project administration (supporting); Resources (lead); Supervision (supporting); Writing – review & editing (supporting). **Andy Thomas:** Project administration (lead); Supervision (lead); Writing – original draft (supporting); Writing – review & editing (equal).

## DATA AVAILABILITY

The data that support the findings of this study are available from the corresponding author upon reasonable request.

## REFERENCES


[1]B. Park, J. Wunderlich, X. Marti, V. Holy, Y. Kurosaki, M. Yamada, H. Yamamoto, A. Nishide, J. Hayakawa, H. Takahashi *et al.*, "A spin-valve-like magnetoresistance of an antiferromagnet-based tunnel junction," Nat. Mater. **10**, 347–351 (2011).

[2]H. Fuke, K. Saito, Y. Kamiguchi, H. Iwasaki, and M. Sahashi, "Spin-valve giant magnetoresistive films with antiferromagnetic Ir–Mn layers," J. Appl. Phys. **81**, 4004–4006 (1997).

[3]G. Anderson, Y. Huai, and M. Pakala, "Spin-valve thermal stability: The effect of different antiferromagnets," J. Appl. Phys. **87**, 5726–5728 (2000).

[4]S. Parkin, K. Roche, M. Samant, P. Rice, R. Beyers, R. Scheuerlein, E. O'sullivan, S. Brown, J. Bucchigano, D. Abraham *et al.*, "Exchange-biased magnetic tunnel junctions and application to nonvolatile magnetic random access memory," J. Appl. Phys. **85**, 5828–5833 (1999).

[5]A. Khvalkovskiy, D. Apalkov, S. Watts, R. Chepulskii, R. Beach, A. Ong, X. Tang, A. Driskill-Smith, W. Butler, P. Visscher *et al.*, "Basic principles of STT-MRAM cell operation in memory arrays," J. Phys. D: Appl. Phys. **46**, 074001 (2013).

[6]W. Zhao, T. Devolder, Y. Lakys, J. Klein, C. Chappert, and P. Mazoyer, "Design considerations and strategies for high-reliable STT-MRAM," Microelectron. Rel. **51**, 1454–1458 (2011).

[7]W. Gallagher, S. Parkin, Y. Lu, X. Bian, A. Marley, K. Roche, R. Altman, S. Rishton, C. Jahnes, T. Shaw *et al.*, "Microstructured magnetic tunnel junctions," J. Appl. Phys. **81**, 3741–3746 (1997).

[8]J. Zhu and C. Park, "Magnetic tunnel junctions," Mater. Today **9**, 36–45 (2006).

[9]S. Yuasa, T. Nagahama, A. Fukushima, Y. Suzuki, and K. Ando, "Giant room-temperature magnetoresistance in single-crystal Fe/MgO/Fe magnetic tunnel junctions," Nat. Mater. **3**, 868–871 (2004).

[10]S. Ikeda, J. Hayakawa, Y. Lee, F. Matsukura, Y. Ohno, T. Hanyu, and H. Ohno, "Magnetic tunnel junctions for spintronic memories and beyond," IEEE Trans. Electron Devices **54**, 991–1002 (2007).

[11]J. Sankey, Y. Cui, J. Sun, J. Slonczewski, R. Buhrman, and D. Ralph, "Measurement of the spin-transfer-torque vector in magnetic tunnel junctions," Nat. Phys. **4**, 67–71 (2008).

[12]A. Tulapurkar, Y. Suzuki, A. Fukushima, H. Kubota, H. Maehara, K. Tsunekawa, D. Djayaprawira, N. Watanabe, and S. Yuasa, "Spin-torque diode effect in magnetic tunnel junctions," Nature **438**, 339–342 (2005).

[13]I. Polenciuc, A. Vick, D. Allwood, T. Hayward, G. Vallejo-Fernandez, K. O'Grady, and A. Hirohata, "Domain wall pinning for racetrack memory using exchange bias," Appl. Phys. Lett. **105**, 162406 (2014).

[14]J. Nogués and I. Schuller, "Exchange bias," J. Magn. Magn. Mater. **192**, 203–232 (1999).

[15]M. Kiwi, "Exchange bias theory," J. Magn. Magn. Mater. **234**, 584–595 (2001).

[16]K. O'grady, L. Fernandez-Outon, and G. Vallejo-Fernandez, "A new paradigm for exchange bias in polycrystalline thin films," J. Magn. Magn. Mater. **322**, 883–899 (2010).

[17]P. Lin, B. Yang, M. Tsai, P. Chen, K. Huang, H. Lin, and C. Lai, "Manipulating exchange bias by spin–orbit torque," Nat. Mater. **18**, 335–341 (2019).

[18]S. Peng, D. Zhu, W. Li, H. Wu, A. Grutter, D. Gilbert, J. Lu, D. Xiong, W. Cai, P. Shafer *et al.*, "Exchange bias switching in an antiferromagnet/ferromagnet bilayer driven by spin–orbit torque," Nat. Electron. **3**, 757–764 (2020).

[19]S. Fukami, C. Zhang, S. DuttaGupta, A. Kurenkov, and H. Ohno, "Magnetization switching by spin–orbit torque in an antiferromagnet–ferromagnet bilayer system," Nat. Mater. **15**, 535–541 (2016).

[20]A. Kurenkov, C. Zhang, S. DuttaGupta, S. Fukami, and H. Ohno, "Device-size dependence of field-free spin-orbit torque induced magnetization switching in antiferromagnet/ferromagnet structures," Appl. Phys. Lett. **110**, 092410 (2017).

[21]J. Kang, J. Ryu, J. Choi, T. Lee, J. Park, S. Lee, H. Jang, Y. Jung, K. Kim, and B. Park, "Current-induced manipulation of exchange bias in IrMn/NiFe bilayer structures," Nat. Commun. **12**, 6420 (2021).

[22]E. Zhang, Y. Deng, X. Liu, X. Zhan, T. Zhu, and K. Wang, "Manipulating antiferromagnetic interfacial states by spin-orbit torques," Phys. Rev. B **104**, 134408 (2021).

[23]X. Chen, A. Hochstrat, P. Borisov, and W. Kleemann, "Magnetoelectric exchange bias systems in spintronics," Appl. Phys. Lett. **89**, 202508 (2006).

[24]S. Tu, T. Ziman, G. Yu, C. Wan, J. Hu, H. Wu, H. Wang, M. Liu, C. Liu, C. Guo *et al.*, "Record thermopower found in an IrMn-based spintronic stack," Nat. Commun. **11**, 1–7 (2020).

[25]O. Gladii, L. Frangou, G. Forestier, R. Seeger, S. Auffret, I. Joumard, M. Rubio-Roy, S. Gambarelli, and V. Baltz, "Unraveling the influence of electronic and magnonic spin-current injection near the magnetic ordering transition of IrMn metallic antiferromagnets," Phys. Rev. B **98**, 094422 (2018).

[26]H. Reichlová, V. Novák, Y. Kurosaki, M. Yamada, H. Yamamoto, A. Nishide, J. Hayakawa, H. Takahashi, M. Maryáko, J. Wunderlich *et al.*, "Temperature and thickness dependence of tunneling anisotropic magnetoresistance in exchange-biased Py/IrMn/MgO/Ta stacks," Mater. Res. Express **3**, 076406 (2016).

[27]W. Meiklejohn and C. Bean, "New magnetic anisotropy," Phys. Rev. **102**, 1413 (1956).

[28]E. Maniv, R. Murphy, S. Haley, S. Doyle, C. John, A. Maniv, S. Ramakrishna, Y. Tang, P. Ercius, R. Ramesh *et al.*, "Exchange bias due to coupling between coexisting antiferromagnetic and spin-glass orders," Nat. Phys. **17**, 525–530 (2021).

[29]X. He, Y. Wang, N. Wu, A. Caruso, E. Vescovo, K. Belashchenko, P. Dowben, and C. Binek, "Robust isothermal electric control of exchange bias at room temperature," Nat. Mater. **9**, 579–585 (2010).

[30]J. Sort, B. Dieny, M. Fraune, C. Koenig, F. Lunnebach, B. Beschoten, and G. Güntherodt, "Perpendicular exchange bias in antiferromagnetic-ferromagnetic nanostructures," Appl. Phys. Lett. **84**, 3696–3698 (2004).

[31]Y. Fan, K. Smith, G. Lüpke, A. Hanbicki, R. Goswami, C. Li, H. Zhao, and B. Jonker, "Exchange bias of the interface spin system at the Fe/MgO interface," Nat. Nanotechnol. **8**, 438–444 (2013).

[32]R. Zhu, W. Zhang, W. Shen, P. Wong, Q. Wang, Q. Liang, Z. Tian, Y. Zhai, C. Qiu, and A. Wee, "Exchange bias in van der Waals $CrCl_3/Fe_3GeTe_2$ heterostructures," Nano Lett. **20**, 5030–5035 (2020).

[33]Z. Wei, A. Sharma, A. Nunez, P. Haney, R. Duine, J. Bass, A. MacDonald, and M. Tsoi, "Changing exchange bias in spin valves with an electric current," Phys. Rev. Lett. **98**, 116603 (2007).
[34]M. Mizuguchi and S. Nakatsuji, "Energy-harvesting materials based on the anomalous Nernst effect," Sci. Technol. Adv. Mater. **20**, 262–275 (2019).
[35]J. Holanda, D. Maior, A. Azevedo, and S. Rezende, "Anisotropic magnetoresistance and anomalous Nernst effect in exchange biased permalloy/(100) NiO single-crystal," J. Magn. Magn. Mater. **432**, 507–510 (2017).
[36]P. Wölfle and T. Ziman, "Theory of record thermopower near a finite temperature magnetic phase transition: IrMn," arXiv:2105.08981 (2021).
[37]W. Lee, S. Watauchi, V. Miller, R. Cava, and N. Ong, "Anomalous Hall heat current and Nernst effect in the $CuCr_2Se_{4-x}Br_x$ ferromagnet," Phys. Rev. Lett. **93**, 226601 (2004).
[38]Y. Pu, D. Chiba, F. Matsukura, H. Ohno, and J. Shi, "Mott relation for anomalous Hall and Nernst effects in $Ga_{1-x}Mn_xAs$ ferromagnetic semiconductors," Phys. Rev. Lett. **101**, 117208 (2008).
[39]D. Kim, P. Syers, N. Butch, J. Paglione, and M. Fuhrer, "Ambipolar surface state thermoelectric power of topological insulator $Bi_2Se_3$," Nano Lett. **14**, 1701–1706 (2014).
[40]F. Ghahari, H. Xie, T. Taniguchi, K. Watanabe, M. Foster, and P. Kim, "Enhanced thermoelectric power in graphene: Violation of the Mott relation by inelastic scattering," Phys. Rev. Lett. **116**, 136802 (2016).
[41]X. Li, L. Xu, L. Ding, J. Wang, M. Shen, X. Lu, Z. Zhu, and K. Behnia, "Anomalous Nernst and Righi-Leduc effects in $Mn_3Sn$: Berry curvature and entropy flow," Phys. Rev. Lett. **119**, 056601 (2017).
[42]S. Watanabe, M. Ohno, Y. Yamashita, T. Terashige, H. Okamoto, and J. Takeya, "Validity of the Mott formula and the origin of thermopower in $\pi$-conjugated semicrystalline polymers," Phys. Rev. B **100**, 241201 (2019).
[43]J. Xu, W. Phelan, and C. Chien, "Large anomalous Nernst effect in a van der Waals ferromagnet $Fe_3GeTe_2$," Nano Lett. **19**, 8250–8254 (2019).
[44]K. Geishendorf, P. Vir, C. Shekhar, C. Felser, J. Facio, J. Brink, K. Nielsch, A. Thomas, and S. Goennenwein, "Signatures of the magnetic entropy in the thermopower signals in nanoribbons of the magnetic Weyl semimetal $Co_3Sn_2S_2$," Nano Lett. **20**, 300–305 (2020).
[45]Y. Chen, Y. Lin, S. Jen, J. Tseng, and Y. Yao, "Effect of Ta seed layer on crystalline structure and magnetic properties in an exchange-biased Co/IrMn system," J. Alloys Compd. **509**, 5587–5590 (2011), https://www.sciencedirect.com/science/article/pii/S092583881100404X.
[46]J. Cho, N. Kim, S. Lee, J. Kim, R. Lavrijsen, A. Solignac, Y. Yin, D. Han, N. Hoof, H. Swagten, B. Koopmans, and C. You, "Thickness dependence of the interfacial Dzyaloshinskii–Moriya interaction in inversion symmetry broken systems," Nat. Commun. **6**, 7635 (2015).
[47]A. Devasahayam and M. Kryder, "The dependence of the antiferromagnet/ferromagnet blocking temperature on antiferromagnet thickness and deposition conditions," J. Appl. Phys. **85**, 5519–5521 (1999).
[48]M. Molina-Ruiz, A. Lopeandia, F. Pi, D. Givord, O. Bourgeois, and J. Rodriguez-Viejo, "Evidence of finite-size effect on the Néel temperature in ultrathin layers of CoO nanograins," Phys. Rev. B **83**, 140407 (2011).
[49]A. Scholl, M. Liberati, E. Arenholz, H. Ohldag, and J. Stöhr, "Creation of an antiferromagnetic exchange spring," Phys. Rev. Lett. **92**, 247201 (2004).
[50]S. Wu, S. Cybart, P. Yu, M. Rossell, J. Zhang, R. Ramesh, and R. Dynes, "Reversible electric control of exchange bias in a multiferroic field-effect device," Nat. Mater. **9**, 756–761 (2010).
[51]S. Sangiao, L. Morellon, G. Simon, J. De Teresa, J. Pardo, J. Arbiol, and M. Ibarra, "Anomalous Hall effect in Fe (001) epitaxial thin films over a wide range in conductivity," Phys. Rev. B **79**, 014431 (2009).
[52]M. Rubinstein, F. Rachford, W. Fuller, and G. Prinz, "Electrical transport properties of thin epitaxially grown iron films," Phys. Rev. B **37**, 8689 (1988).
[53]C. Cirillo, C. Barone, H. Bradshaw, F. Urban, A. Di Bernardo, C. Mauro, J. Robinson, S. Pagano, and C. Attanasio, "Magnetotransport and magnetic properties of amorphous $NdNi_5$ thin films," Sci. Rep. **10**, 13693 (2020).
[54]N. Nagaosa, J. Sinova, S. Onoda, A. MacDonald, and N. Ong, "Anomalous hall effect," Rev. Mod. Phys. **82**, 1539 (2010).
[55]R. Ramos, T. Kikkawa, K. Uchida, H. Adachi, I. Lucas, M. Aguirre, P. Algarabel, L. Morellón, S. Maekawa, E. Saitoh *et al.*, "Observation of the spin Seebeck effect in epitaxial $Fe_3O_4$ thin films," Appl. Phys. Lett. **102**, 072413 (2013).
[56]N. Mott, H. Jones, H. Jones, and H. Jones, *The Theory of the Properties of Metals and Alloys* (Courier Dover Publications, 1958).
[57]S. Guin, P. Vir, Y. Zhang, N. Kumar, S. Watzman, C. Fu, E. Liu, K. Manna, W. Schnelle, J. Gooth *et al.*, "Others zero-field Nernst effect in a ferromagnetic Kagome-lattice Weyl-semimetal $Co_3Sn_2S_2$," Adv. Mater. **31**, 1806622 (2019).
[58]L. Ding, J. Koo, L. Xu, X. Li, X. Lu, L. Zhao, Q. Wang, Q. Yin, H. Lei, B. Yan *et al.*, "Intrinsic anomalous Nernst effect amplified by disorder in a half-metallic semimetal," Phys. Rev. X **9**, 041061 (2019).
[59]D. MacDonald, *Thermoelectricity: An Introduction to the Principles* (Courier Corporation, 2006).
[60]P. Ritzinger, H. Reichlova, D. Kriegner, A. Markou, R. Schlitz, M. Lammel, D. Scheffler, G. Park, A. Thomas, P. Středa *et al.*, "Anisotropic magnetothermal transport in $Co_2MnGa$ thin films," Phys. Rev. B **104**, 094406 (2021).